Open Research Online

Neutron diffraction residual stress measurements on girth-welded 304 stainless steel pipes with weld metal deposited up to half and full pipe wall thickness

Journal Item

For guidance on citations see FAQs.

oro.open.ac.uk

Accepted Manuscript

Neutron diffraction residual stress measurements on girth-welded 304 stainless steel pipes with weld metal deposited up to half and full pipe wall thickness

R.D. Haigh, M.T. Hutchings, J.A. James, S. Ganguly, R. Mizuno, K. Ogawa, S. Okido, A.M. Paradowska, M.E. Fitzpatrick
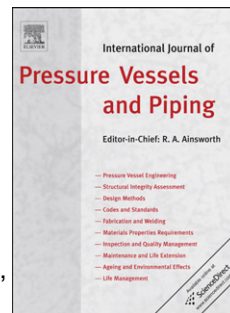
Please cite this article as: Haigh RD, Hutchings MT, James JA, Ganguly S, Mizuno R, Ogawa K, Okido S, Paradowska AM, Fitzpatrick ME, Neutron diffraction residual stress measurements on girth-welded 304 stainless steel pipes with weld metal deposited up to half and full pipe wall thickness, *International Journal of Pressure Vessels and Piping* (2012), doi: 10.1016/j.ijpvp.2012.08.003.

- 304 steel girth welded with weld metal to half and full pipe wall thickness

- Residual stresses measured by neutron and X-ray diffraction, and modelled by FE

- Weld toe residual σ_{hoop} changes from tensile to compressive from half to fully-filled

- FE model for the fully-filled weld gives higher stress levels than those measured

- Discrepancy is attributed to the isotropic hardening model used

Neutron diffraction residual stress measurements on girth-welded 304 stainless steel pipes with weld metal deposited up to half and full pipe wall thickness

R. D. Haigh[1], M. T. Hutchings[1], J. A. James[1], S. Ganguly[1], R. Mizuno[2], K. Ogawa[3], S. Okido[4], A. M. Paradowska[5], M. E. Fitzpatrick[1,*]

[1] *Materials Engineering, The Open University, Walton Hall, Milton Keynes, MK7 6AA, UK*

[2] *Nondestructive Evaluation Center, Japan Power Engineering and Inspection Corporation, 14-1, Benten-cho, Tsurumi-ku, Yokohama, 230-0044 Japan*

[3] *Aging and Material Reliability Evaluating Group, Nuclear Energy System Safety Division, Japan Nuclear Energy Safety Organization, TOKYUREIT, Toranomon Building, 17-1, Toranomon 3-chome, Minato-ku, Tokyo, 105-0001, Japan*

[4] *Material, Strength and Reliability Unit, Department of Material Research for Power Plants, Hitachi Research Laboratory, Hitachi, Ltd. 3-1-1, Saiwai-cho, Hitachi-shi, Ibaraki, 317-8511, Japan*

[5] *ISIS Facility, STFC Rutherford Appleton Laboratory, Chilton, Didcot OX11 0RA, UK*

*Corresponding author. m.e.fitzpatrick@open.ac.uk. Tel: +44 1908 653100

Abstract

The residual stress distribution has been measured in two girth-welded austenitic stainless steel pipe weldments using time-of-flight neutron diffraction. One had weld filler metal deposited up to half the pipe wall thickness, and one had weld metal deposited up to full pipe wall thickness. The aim of the work is to evaluate the evolution in residual stress profile on filling the weld, on which there is little experimental data, and where the selection of the correct hardening model used in finite element modelling can benefit greatly from an understanding of the intermediate residual stresses partway through the welding operation. The measured residual stresses are compared with those calculated by finite element modelling and measured using X-ray diffraction. The results show a change in the measured hoop stress at the weld toe from tension to compression between the half-and fully-filled weld. The finite element results show an overprediction of the residual stress, which may be a consequence of the simple isotropic hardening model applied. The results have implications for the likely occurrence of stress corrosion cracking in this important type of pipe-to-pipe weldment.

1. Introduction

The primary area of component cracking in power plant piping is at welded joints [1]. One of the main causes of failure in welded pipes is stress corrosion cracking (SCC), and the likelihood of this occurring is highly dependent on residual stresses present in the weld region, particularly if there are surface tensile stresses in regions exposed directly to coolant or condensate.

Prediction of the magnitude and profile of the residual stress distribution in coolant pipe work is extremely difficult, and experimental validation of finite element-based models of residual stress generation is required [2]. There are complex interactions

between heat input and the geometry of a particular assembly that control the location and magnitude of the final residual stresses [3], and the detailed variation of the residual stresses near component surfaces where defects may be present is particularly important in affecting component life [4].

Neutron diffraction techniques are a powerful means for the non-destructive in-depth determination of residual stresses. By fabrication of plant-scale mock-ups using controlled fabrication conditions, experimental samples can be provided in which the fabrication history is well-defined. Measurement of such samples can provide knowledge of the residual stresses arising from thermal histories during welding. During the cool down and solidification following a weld pass deposition, molten material will shrink and tend to pull all other material with it. In the case of butt-welded pipe weldments this manifests itself as a circumferential contraction about the girth weld. The parent metal near to the heat-affected zone (HAZ) will partially resist the deformation, and it is this partial resistance or partial flow which results in residual stresses. After welding, tensile residual stresses usually develop in both the weld metal and the heat-affected zone (HAZ) metal. The magnitude of the residual stress field is affected by the pipe's diameter, its thickness and the size of the weld bead; as well as factors such as the weld heat input, number of passes, and the mechanical properties of the parent and weld material. Successive weld passes, in a multi-weld pass weld, will result in a cyclic accumulation of both residual elastic stresses and plastic strains. Girth weld beads generally lead to high tensile residual stresses on the inside surface of the pipe [5]. In particular it is tensile residual stresses in the HAZ which are considered to cause SCC.

Finite element modelling (FEM) studies on weld root stresses and the effect of the number of weld passes have previously been made in welded ANSI 304 stainless steel pipes with a diameter of 320 mm and thickness of 10 mm [6]. The results suggested that axial and hoop stresses are highly tensile up to 20 mm from the weld centre line in the HAZ, where SCC is anticipated. A lower number of weld passes was predicted to result in higher axial tensile stresses in the HAZ, but not in the weld, on the inner pipe surface.

In the work presented here the residual stress distribution throughout the weld area has been measured using time-of-flight neutron diffraction for two specially-fabricated girth-welded austenitic stainless steel pipes. One had weld metal deposited up to half the pipe wall thickness, and one with weld metal deposited up to full pipe wall thickness. There are two aims of the current work: firstly to evaluate the change in stress profile on filling the weld, on which there is little current experimental data. Secondly, to validate an FE model of the welded pipes, developed to predict the change in the stress profile on filling the weld. The residual stress distributions measured using neutron diffraction are compared with those calculated by finite element modelling, and with the results of near-surface measurements using X-ray diffraction. Hardness and grain size measurements are also reported.

2. Experimental details

2.1 The weldment samples

Two girth-welded pipe weldments were fabricated using type 304 austenitic stainless steel, with dimensions of 305 mm outer diameter, 25 mm wall thickness and 500 mm length. Each weldment was formed by TIG welding two pipe sections together. Multi-pass weld layers were deposited into the groove between the two pipe sections. Weld passes were made until filler material either half- (11 passes), or fully- (33 passes) filled the grooves in the two weldments. The sequence of weld passes is shown in Figure 1. The chemical compositions of the pipe parent and weld filler metals are given in Table 1. The multi-pass layers were deposited by the gas-tungsten-arc (GTAW) method. Weld beads were deposited at a continuous speed of 9 cm/min, a voltage of 10 V, a current of 130-170 A and a wire feed speed of 50-80 cm/min.

In order to define the positions at which the residual strain was measured, and the residual stress calculated, coordinate axes were defined as shown in Figure 2. The origin is taken as the centre of the pipe, and positive and negative x, y and z directions are defined in the figures. All dimensions are in units of mm. A reference point defined as top dead centre (TDC, labelled as "T") is located at the position $x = -250$, $y = 0$, $z = 140$. There are reference azimuthal angles α engraved around the weldment at the opposing end of the weldment from the TDC end, that is at positive $x \approx 250$. The TDC was located at a $\alpha = 0°$. All measurements reported here were taken at $\alpha = 180°$, that is in the x-z plane with $y = 0$. An alternative co-ordinate system, which is used in some descriptions of the positions in the weldment, uses cylindrical co-ordinates r, α, x, where r is the radius from the x axis. So that at $\alpha = 180°$, $y = 0$ and $r = -z$. The results are presented for positions through the thickness given in terms of the co-ordinate x and the radial distance, $t = (r - r_i)$, where r_i is the radial position of the tip of the weld's innermost surface. In the case of the half-filled and fully-filled weldments r_i is taken as 125.57 and 123.61 respectively. During fabrication the welding passes were made around the recess in the direction along the axial direction from negative to positive x as defined in Figure 2.

In order to facilitate neutron measurements, by reducing the total path traversed by the neutron beam, both weldments had an 80×160 mm^2 access aperture cut in the negative y direction as shown in Figure 2. This aperture is centred at $\alpha = 90°$, at $x = 0$, $y = -140$, $z = 0$. The material removed to form this aperture was used to provide stress-free reference cubes as described below.

2.2 Neutron diffraction measurements

The neutron diffraction measurements were made using the ENGIN-X time-of-flight (TOF) instrument operating at the ISIS spallation neutron source at the UK Rutherford-Appleton Laboratory. Details of this instrument are given in [7, 8]. The polychromatic neutron beam enters the instrument from a neutron guide through an incident slit aperture which, along with focusing slit apertures before the two detectors, defines the volume of sample probed. This is called the measurement gauge volume (GV) of the instrument, and the sample is positioned so that the position at which the strain is to be measured is at the GV centre. The beam diffracted from that part of the sample in the gauge volume enters two detector banks at 90° on either side

of the incident beam. The TOF technique allows for simultaneous measurement of many diffraction peaks, and the diffraction pattern obtained is subsequently analysed using a Rietveld or Pawley refinement of a selection of the peaks obtained, in combination with the known cubic crystal lattice structure, to give a mean value of the lattice parameter *a* within the gauge volume [9, 10]. From this measured lattice parameter *a* in the sample weldment, and that of a 'stress-free' sample, a_0, the elastic lattice strain may be calculated. The strain component measured is that in the direction of the scattering vector **Q**, which bisects the angle between the incident and diffracted beams. With diffracted beams measured in two detectors at 90° two strain components at 90° can therefore be measured. In the present measurements two sets of focusing collimators were used before the detectors, with corresponding incident slit apertures, to define gauge volumes of $3 \times 3 \times 3 mm^3$ and $4 \times 4 \times 4 mm^3$.

Alpha iron powder (Goodfellow LS119266 J H FE006020/6 with 60 μm particle diameter and 99 % purity) was used for the calibration of the measurements and to correct differences between the two detector banks. As changing from a GV of $3 \times 3 \times 3$ to $4 \times 4 \times 4 mm^3$ required collimator changes, the Fe powder was measured for each gauge volume. A CeO_2 powder, used on the ENGIN-X instrument as an experimental standard, was also measured.

Residual strain components were measured in the hoop, radial and axial directions, which are assumed to be the principal stress component directions. Each weldment was therefore mounted on the instrument sample table in one of two orientations. With the pipe weldment axis in the vertical configuration (as shown in Figure 3) radial and hoop components are measured. In this orientation the positive x-axis pointed upwards, with the TDC at the bottom. In order to determine the axial component the pipe weldment was aligned with its axis horizontal along the scattering vector **Q**, when in principle the radial component can also be measured. However because of space constraints it was necessary to remove the collimator from Bank 1 for the axial strain measurements; consequently, only these were measured on Bank 2. The detectors used to measure the three strain components are summarised in Table 2.

In order to accurately position the weldments on the instrument, the SScanSS experimental design and visualization software [11] was used. A map of the surface of the weldment was first scanned off-line using a Scan Shark V5 laser probe mounted on a portable scanning CimCore Infinite II arm. The laser probe was connected to a Perceptron 4SightM imaging computer which in turn was connected to a PC. Laser scanned images were processed with the PowerInspect routine. The surface scan was recorded relative to fiducial points, which were spheres attached to the outside of the weldments. The required positions of measurement were defined relative to these points. In this way allowance was made for the distortion of the weld area of the weldments, shown in the laser-scanned cross sections in Figure 4. The fiducial points were used to position the weldment on the instrument using theodolites and robot probes which had been calibrated to point accurately to the centre of the instrumental gauge volume. The required positions of measurement of an irregular object, such as the weldment in the region of the weld, can then be very accurately positioned at the centre of the GV by orthogonal translation slides, two horizontal and one vertical, under the instrument sample table.

2.3 Positions of strain measurement in the weldment

The location of the positions of strain measurement in each weldment is shown in Figure 4, where the measurement positions have been marked as stars superimposed on images obtained by laser-scanned cross sections of the deformed weldments. The position of the fusion boundaries have been marked for clarity. The measurement points were adjusted to be along 'lines' with each point equidistant from the inside pipe surface, taking into account the welding distortion. Scans of measured strain were made at positions along the axial direction x along these lines.

$3 \times 3 \times 3$ mm^3 and $4 \times 4 \times 4$ mm^3 gauge volumes were selected for strain mapping, the smaller gauge volume being used for regions of most interest. To avoid partial filling of the neutron gauge volume near the surface, which can lead to anomalous strain effects [12], the points were measured no nearer than 2.3 and 3.0 mm from the external pipe surfaces for the smaller and larger gauge volumes respectively. The smaller gauge volume allowed for both higher spatial resolution strain measurement in the weld-HAZ region and for measurements to be made nearer to the weldment's inner surface. As far as possible the $3 \times 3 \times 3$ mm^3 gauge volume was used to measure strains in the weld-HAZ region of the half-filled weldment, but due to a shortage of experimental time it was not possible to complete the mapping of this weldment with this gauge. Consequently, in the half-filled weldment the weld-HAZ region strain mapping was completed with a $4 \times 4 \times 4$ mm^3 gauge volume. The positions of the points with the two gauge volume are marked in Figure 4.

2.4 Stress-free cube calibration

In determining the residual strain, and thence stress, one of the most important parameters to determine is the variation of the stress-free, or strain-free, lattice parameter a_0, to which the shift in measured lattice parameter in the weldment is referred. Changes in stress-free lattice parameter can occur because of changes in the solute content of the lattice owing to the thermal cycling of the parent material in the HAZ, and compositional changes due to the addition of filler material, if present, in the weld itself. The measured strains are therefore highly-dependent on accurate knowledge of any stress-free lattice parameter variation with position in the weldment.

The stress-free lattice parameter was determined from small cubes cut from areas in each weldment, in which all macrostrain is assumed to be removed. However *a priori* there may be microstrains, in particular plastically-induced intergranular strains, present in these cubes, which may be anisotropic. In order to determine the macrostrain one must therefore subtract from the measured lattice parameter in the weldment the stress-free lattice parameter at the same position and orientation. In this way any microstrains present in both will cancel, and the difference will reflect only the macrostrain. However in the present case of the use of a time-of-flight diffraction pattern to determine an average lattice parameter from many diffraction peaks, it has been shown that the elastic anisotropy and plastically-induced intergranular microstrain is averaged out, and that the stress may be determined from the strains using the macroscopic elastic constants [9].

The cubes were extracted, by EDM cutting, from the section of each weldment cut to provide the access slots. Parent metal cubes were cut 80 mm away from the weld; and HAZ and weld metal cubes near the weld root immediately adjacent to the weld and from the weld root itself respectively. These locations are shown in Figure 4, and

summarised in Table 3. Care was taken to ensure that the cubes were cut along radial lines with respect to the axis of the pipe. In each case small cubes were first cut with dimensions of $3 \times 3 \times 3$ mm^3, marking the orientation of each relative to the weldment in different colours. These were then glued together, maintaining their orientation, into blocks of eight, with dimensions of $6 \times 6 \times 6$ mm^3. When carefully positioned at the GV centre they filled the gauge volume thus avoiding spurious edge effects.

All the cubes were measured in the two orientations summarised in Table 2, so that the strains in the hoop direction were measured using both detectors. Following observations of some apparent differences in the a_0 values determined in different experimental sessions, that were greater than the expected statistical uncertainties, it was decided to use the a_0 measured in the same detector, and same orientation, as a was measured in the weldment, for each material. The value of a_0 measured with the same gauge volume as was used to measure a for each position in Figure 4 was used to calculate the strain.

2.5 Determination of strain and stress

The principal strain and stress directions have been assumed to lie along the axial, hoop and radial directions of the weldments. Using the value of a found from a Pawley fit to five diffraction peaks (222, 311, 220, 200 and 111), and the corresponding values of a_0, the strain components at each measurement position were determined. These strain components were converted to the corresponding stress component using the bulk material elastic constants $E = 209$ GPa, and $\nu = 0.30$ [13].

Data are presented here in the form of contour maps of stress in Figures 5 to 10. The position of both the fusion boundary and the weldment cross section, obtained from laser scans of the weld-deformed weldments, are superimposed on the maps. Figures 5 to 7 are macro-sections where the position of the measurement points are shown in Figure 4 (i) and (ii). Figures 8 to 10 are detailed maps of the weld region where the position of the measurement points is shown in Figure 4 (iii) and (iv).

2.6 Hardness

A hardness map was made on polished cross-sections of material taken from the neutron access slots in the half-filled and fully-filled weldments. The cross-sections were ground and polished until reflective. The Vickers hardness was measured using a Struers Duramin-A300 hardness tester equipped with a computer-controlled stage. Points were measured with 5 kg force applied for 5 s, on a 5×1 mm^2 grid in the ranges $-60 \leq x \leq -15$ and $15 \leq x \leq 60$. Points were also measured with a 5 kg force for 5 s on a 1×1 mm^2 grid in the range $-15 \leq x \leq 15$. The results are shown in Figure 11.

3 Results

3.1 Neutron diffraction measurements

Contour maps of the axial, hoop and radial stress components determined from the full range of the neutron diffraction data are shown in Figures 5 to 7. The weld centre line is taken as $x = 0$. The results for the fully-filled weldment are shown above those for the half-filled weldment so that the comparison of stress profiles can be more

clearly seen. As an approximation, maps are interpolated between measured points, and no extrapolation between the outermost points and the sample surface boundary has been undertaken. Therefore there is a small gap between the top and bottom of the maps and the inner or outer pipe surface boundaries respectively. The comparison in the inner region of the weld, where more closely spaced measurement points were made is shown in more detail in Figures 8 to 10.

3.1.1 The half-filled weldment

The maps of stresses shown in Figures 5b-7b are quite symmetrical about the weld centre line $x = 0$ for all three components. The axial stress component is compressive near the inner surface, less so in mid-depth, but becomes tensile towards the outer surface. The hoop stress component shows a wide variation through the wall thickness. It is compressive in the HAZ and away from $x = 0$, but near the inner surface and at mid-thickness peaks in tension in the region of $x = 0$. The radial stress component shows least variation with axial co-ordinate x, and is generally low and compressive. These findings are broadly supported by the more detailed maps in Figures 8b-10b.

3.1.2 The fully-filled weldment

The stress maps obtained in the fully-filled weldment, shown in Figures 5a-7a and 8a-10a, are again generally symmetric for the axial and radial components, whereas the hoop component shows a tensile peak off centre. The axial stress component varies only slightly with x near the inner surface and is compressive. It shows a tendency to peak compressively at mid thickness, but becomes tensile towards the outer edge. The hoop stress component shows the greatest variation with x. Near the inner surface it is compressive, exhibiting a sharp compressive peak in the weld region. However in the weld region it becomes more tensile as the radius increases and shows a strong off-centre tensile peak at positive x towards the outer surface. The radial stress component shows less variation with x and is compressive near the inner surface becoming weakly tensile near the outer surface.

3.2 Vickers hardness

Vickers hardness maps were determined in both weldments, and are shown in HV units in Figures 11a and b. The hardness of a hot worked metal, such as a stainless steel subject to welding, increases with residual plastic strain, and therefore hardness mapping may be indicative of plastic strain history. It is interesting to note that peak hardness, and by implication peak plastic strain, occurs in the HAZ immediately adjacent to the fusion boundary in both weldments, and that the values are most intense near the inner weldment surface.

3.3 Finite Element modelling

Finite element modelling of the residual stresses was performed for both the half-filled and fully- filled weldments using Abaqus® (Standard v 6.2.6.) software. The model was a 2D axially-symmetric temperature-dependent model, with material cyclic plastic behaviour based on the isotropic hardening rule.

The overall shape of the deposited area was determined by the observed cross section, but the shapes of each individual weld pass were idealised as rectangular in the model. The entire weld sequence was simulated, with the heat input simulated for each welding pass.

The mechanical melting point is one of the factors that influence the residual stress distribution. A sensitivity analysis for the mechanical melting point (the "annealing temperature" in Abaqus) was performed, and the analytic result of 800°C was found to be in best agreement with previous experimental results for type 304 austenitic stainless steel. Above this temperature little residual stress is generated because of the reduction in yield stress.

The results for the axial and hoop stress components in the half-filled weldment are shown in Figures 12a and b. The corresponding maps for the fully-filled weldment are shown in Figure 13a and b. Both Figures 12 and 13 have the same axes as defined in Figure 2 and can be directly compared with Figures 5 to 10.

The calculated stress distribution of axial tensile stress component in the half-filled weldment, shown in Figure 12a, exhibits a peak of 200 MPa in the lower part of the weldment. There is a predicted peak compressive stress of –200 MPa near the top of the weld. A maximum tensile hoop stress component of 550 MPa is predicted at the weld root, shown in Figure 12b, and 250 MPa at the top of the weld. There are compressive stresses of –250 MPa at x = ± 25 mm.

The stress patterns for the fully-filled weldment shown in Figures 13a and b are symmetrical near the inner surface, but the calculations show an off-centre tensile peak into the HAZ at about two thirds of the thickness in both axial and hoop components. This off-centre peak is the on the same side as the final weld passes, that is in the positive *x* direction, and is around 300 MPa for the axial stress component and higher at around 700 MPa for the hoop stress component. In the case of the axial stress component there is a tensile maximum at the weld toe and a compressive dip of around –350 MPa along the weld axis.

3.4 Measurement of near-surface stress by the X-ray technique

Experimental measurements of the near-surface residual stress on the fully-filled weldment were undertaken using the X-ray $\sin^2\psi$ technique. Results for the axial and hoop stress components at the outer surface are shown in Figure 14 a and b, and those for the hoop stress component at the inner surface are shown in Figure 15. The measurements were made at 90º intervals in the angle α around the circumferential weld. Those data taken at α = 180º correspond to the centreline position of the residual stresses measured in depth by neutron diffraction.

The data show a tensile peak stress with *x* in the HAZ on either side of the weld, but a lower stress in the weld region itself. The peaks are more pronounced for the hoop stress component near the outer surface. However at the inner surface the variation with *x* is small, and the stress generally low.

4. Discussion

A comparison of the neutron diffraction data with the FE model results shows good agreement in the general pattern of stress in both weldments. However the FE predicted stress levels tend to be higher than those measured, particularly in the case of the fully-filled weldment. It is likely that a kinematic or mixed hardening model rather than the isotropic hardening model used in the assessments might reduce these predicted levels. The predicted change from tensile to compressive hoop stress component between half-filled and fully filled welds is in agreement with the

measurements, as is the tensile off-centre peak at two thirds of the thickness in the latter.

In the case of the half-filled weldment, the FE prediction of the axial stress component is relatively weak (Figure 12a), in agreement with the measurements, but the trend is not close to that measured (Figures 5b and 8b). The calculated hoop stress component shown in Figure 12b agrees qualitatively with the neutron diffraction results of Figures 6b and 9b. For both components the FEM predictions for the half-filled weldment are larger by ~100 MPa compared to the measured data.

In the case of the fully-filled weldment the maximum predicted peak stress of 700 MPa in Figure 13b seems a little higher than normally expected in a pipe weldment. The trends in both axial and hoop stress components through the weld thickness, and along the axis of the weldment, are generally quite similar. Of particular significance is the agreement of the off-centre stress peak in the tensile hoop stress component for the fully-filled weldment between FEM and neutron diffraction . The FEM predicts a similar peak for the axial component, but this has not been observed experimentally. Away from the weld and HAZ area there is quite good agreement of the FE model and the neutron diffraction data for both the axial and hoop stress components over the region of measurement.

The measurements and calculations for positions close to the weld centre, and near the inner surface, are compared in graphical form in Figure 16. This shows the general points made above. In the case of the axial component, the half-filled weldment data agree well but for the fully filled weldment the FEM shows higher stress levels. The hoop components show similar trends in both weldments, but again the FEM stress levels are higher. Both exhibit the change from hoop tensile to compressive stress in this region as the weld is filled.

Dong [14] describes two characteristic residual stress distributions: bending-dominated and self-equilibrated. The two types are influenced by parameters of pipe radius, thickness, and weld pass sequence. In our welded pipe geometry the self-equilibrated type would be expected due to the relatively small radius, and our measured and analysed data show the trend of self-equilibrated type residual stress.

From the results one can speculate that for a the fully-filled weldment in a real plant component the presence of a compressive hoop stress component toward the HAZ near the weld root is likely to inhibit crack formation in this region, and thereby SCC in the hoop direction. Although never used in practice, the tensile hoop stress component near the weld root of the half-filled weldment indicates a susceptibility to SCC in the hoop direction in such a weldment.

The X-ray data, while not comparable directly to the neutron data because of the different measurement location, confirm a tensile stress in the hoop component near the outer surface, with compressive stress near the inner weld toe in the fully-filled weldment.

The hardness measurements show higher levels in the weld root and HAZ than elsewhere. If interpreted as an indication of plastic strain this will be highest in these regions.

Conclusions

1. Neutron diffraction has been applied successfully to measure the residual strains, and thereafter to calculate the stresses, in two welded pipe samples in which the groove between the pipes was half- and fully-filled with weld. The measured stress profiles have been compared with assessment of the stress from finite element calculations, and with near surface measurements made by the X-ray technique.

2. There is a very marked change in the variation with axial position of the hoop stress component between the half-filled and fully-filled weld (Figures 6 and 9). The hoop stress changes near the inner weld region, that is the toe of the weld, from tensile hoop stress in the half-filled weldment to a compressive hoop stress for the fully-filled weldment. The axial stress component shows a similar but smaller change.

3. Possible levels of plastic strain were determined indirectly by hardness measurements. Peak hardness, and by implication peak plastic strain, occurs in the HAZ immediately adjacent to the fusion boundary in both half- and full-filled weldments, with the highest hardness near the inner pipe surface.

4. The X-ray data, while not comparable directly to the neutron data because of the different measurement location, confirm a tensile stress in the hoop component near the outer surface, with compressive stress near the inner weld toe in the fully-filled weldment.

5. The FE assessment for the fully-filled weldment gives higher stress levels than those measured, particularly for the hoop component. However the general stress pattern predicted is generally similar to those measured for both weldments. It is possible that the overestimate is due to the isotropic hardening model used.

Acknowledgements

Figure captions

Figure 1: The sequence of weld passes in the half-filled, 11 passes, and fully filled, 33 passes, weldments. The axial coordinate x is zero at the weld centre and increases from left to right.

Figure 2: Right-hand coordinate system used, with top-dead-centre (TDC, labelled as "T") in the –x direction, and the –y direction passing through the access hole that was machined in the sample to reduce the neutron path length. The origin of the coordinate system is at the centre of the weldment, i.e. at the intersection of the pipe axis with the plane passing through the centre of the weld groove. Measurements made with the weldment in the vertical position had the TDC fiducial point downwards, (iii) is then looking upwards towards positive x.

Figure 3 The half-filled weldment in the vertical orientation on the ENGIN-X instrument, allowing for measurement of the hoop and radial strain components. The fiducial spheres on the sample can be seen.

Figure 4 Map of the measurement positions: (i) and (iii) for the fully-filled weldment and (ii) and (iv) for the half-filled weldment. Most points were measured with a $4 \times 4 \times 4$ mm^3 GV; however where points are encased in a dotted rectangle a $3 \times 3 \times 3$ mm^3 GV was used. Relative positions of cubes taken to determine d_0 are marked with squares labelled as a, b and c for parent, weld and HAZ material respectively.

Figure 5 A contour map of the axial stress component, in MPa. (a) measured in the fully-filled weldment. (b) measured in the half-filled weldment. Measurement positions are marked by crosses.

Figure 6: A contour map of the hoop stress component, in MPa. (a) measured in the fully-filled weldment. (b) measured in the half-filled weldment. Measurement positions are marked by crosses.

Figure 7: A contour map of the radial stress component, in MPa. (a) measured in the fully-filled weldment. (b) measured in the half-filled weldment. Measurement positions are marked by crosses.

Figure 8: Detailed contour map of the axial stress component in MPa over the region close to the weld axis $x = 0$. (a) measured in the fully-filled weldment. (b) measured in the half-filled weldment. Measurement positions are marked by crosses.

Figure 9: Detailed contour map of the hoop stress component in MPa over the region close to the weld axis $x = 0$. (a) measured in the fully-filled weldment. (b) measured in the half-filled weldment. Measurement positions are marked by crosses.

Figure 10: Detailed contour map of the radial stress component in MPa over the region close to the weld axis $x = 0$. (a) measured in the fully-filled weldment. (b) measured in the half-filled weldment. Measurement positions are marked by crosses.

Figure 11 Contour map of the hoop Vickers hardness in HV5/5 units. Images were measured over the weld region along the -axis. (a) measured in the fully-filled weldment. (b) measured in the half-filled weldment

Figure 12 Contour map of (a) axial stress and (b) hoop stress components in MPa for the half-filled weldment by FEM analysis

Figure 13 Contour map of (a) axial and (b) hoop stress components in MPa for the fully-filled weldment assessed by FEM analysis

Figure 14 Results of surface X-ray measurements made on the outer pipe surface of the fully-filled weldment. The variation along x of (a) the axial stress component (b) the hoop stress component.

Figure 15 Results of surface X-ray measurements made on the inner pipe surface of the fully-filled weldment. The variation along x of the hoop stress component.

Figure 16 Comparison between the results of neutron diffraction measurements and Finite Element Model calculations of residual stress components in the half-filled (HFP) and fully filled (FFP) weldments. The data are for positions close to the weld centre near the inner surface. The abscissa is the co-ordinate x.

References

[1] Edwards L, Smith MC, Turski M, Fitzpatrick ME, Bouchard PJ. Advances in Residual Stress Modeling and Measurement for the Structural Integrity Assessment of Welded Thermal Power Plant. Advanced Mater Res. 2008;41-42:391-400.

[2] Dong P, Hong JK. Recommendations for determining residual stresses in fitness-for-service applications. WRC Bulletin. 2002:1-161.

[3] Bouchard PJ. The NeT bead-on-plate benchmark for weld residual stress simulation. International Journal of Pressure Vessels and Piping. 2009;86:31-42.

[4] Bouchard PJ. Validated residual stress profiles for fracture assessments of stainless steel pipe girth welds. International Journal of Pressure Vessels and Piping. 2007;84:195-222.

[5] Basavaraju C. Simplified Analysis of Shrinkage in Pipe to Pipe Butt Welds. Nuclear Engineering and Design. 2000;197:239-47.

[6] Sattari-Far I, Farahani MR. Effect of the weld groove shape and pass number on residual stresses in butt-welded pipes. International Journal of Pressure Vessels and Piping. 2009;86:723-31.

[7] Dann JA, Daymond MR, Edwards L, James JA, Santisteban JR. A Comparison between Engin and Engin-X, a new diffractometer optimized for stress measurement. Physica B. 2004;In press.

[8] Santisteban JR, Daymond MR, James JA, Edwards L. ENGIN-X: a third generation neutron strain scanner. J Appl Crystallography. 2006;39:812-25.

[9] Daymond MR, Bourke MAM, Dreele RBV, Clausen B, Lorentzen T. Use of Rietveld Refinement for Elastic Macrostrain Determination and for Evaluation of Plastic Strain History from Diffraction Spectra. J Appl Phys. 1997;82:1554-62.

[10] Rietveld HM. Line Profiles of Neutron Powder-Diffraction Peaks for Structure Refinement. Acta Cryst. 1967;22:151-2.

[11] James JA, Edwards L. Application of robot kinematics methods to the simulation and control of neutron beam line positioning systems. Nuclear Instr Methods in Physics Res A. 2007;571:709-18.

[12] Edwards L. Near-surface stress measurement using neutron diffraction. In: Fitzpatrick ME, Lodini A, editors. Analysis of Residual Stress using Neutron and Synchrotron Radiation. London: Taylor & Francis; 2003. p. 233-48.

[13] Hutchings MT, Withers PJ, Holden TM, Lorentzen T. Introduction to the Characterisation of Residual Stress by Neutron Diffraction. London: Taylor & Francis; 2005. p. 241.

[14] Dong P. On the Mechanics of Residual Stresses in Girth Welds. Journal of Pressure Vessel Technology. 2007;129:345-54.

	Composition / wt %							
	C	Si	Mn	P	S	Ni	Cr	Fe
Filler (Weld) Metal	0.012	0.44	2.05	0.021	<0.001	9.7	19.54	68.23
Pipe (Parent) Metal	0.010	0.42	1.49	0.019	–	9.15	18.19	70.72

Table 1: The chemical composition of the pipe parent material and the filler weld metal

Sample	Bank 1	Bank 2
Weldments	Radial	Hoop
		Axial
Cubes: orientation 1	Radial	Hoop
Cubes: orientation 2	Hoop	Axial

Table 2 Detectors used to measure strain components in the weldments and the stress-free cubes.

		Position in cylindrical coordinates (r, α, x)	
Material sampled	Location	Fully-filled weldment	Half-filled weldment
Parent	Mid wall	(129.04 ,90±5°, –63.0)	(128.9, 90±5°, –52.0)
HAZ	Inside Edge	(126.18, 90±5°, 7.5)	(128.08, 90±5°, 5.0)
Weld	Inside Edge	(139.54±11.0, 95°, 0.0)	(139.4±11.0 ,95°, 0.0)

Table 3 The locations in the original weldments, shown in Figure 3, at which the stress free cubes were cut. All positions are expressed in terms of cylindrical coordinates where values for *r* and *x* are given in mm. The coordinate system is defined in Figure 2.

33passes, 11layers

11passes
5layers

(i)

(iii)

a

t=0

(ii)

(iv)

a

t=0

25 mm

t

+x

x=0

b   c

b   c

25 mm

(a) Axial Stress Map

(b) Axial Stress Map

(a) Hoop Stress Map

(b) Hoop Stress Map

(a) Radial Stress Map

(b) Radial Stress Map

(a) Axial Stress Map

(b) Axial Stress Map

(a) Hoop Stress Map

(b) Hoop Stress Map

(a) Radial Stress Map

(b) Radial Stress Map

(a) Hoop Hardness Map

(b) Hoop Hardness Map

Condition of x-ray measurement
Slit size : φ 3mm
φ angle : ±26 deg with ±4 deg oscillation

Condition of x-ray measurement
Slit size : φ 3mm
φ angle : ±24 deg with ±4 deg oscillation

Out put line of analysis

	N.D. measure	FEM analysis
HFP	·····■·····	—
FFP	·····■·····	—

Weldmetal

Hoop stress (MPa)

Distance from weld center line (mm)

Hoop stress

Weldmetal

Axial stress (MPa)

Distance from weld center line (mm)

Axial stress